SIAM J. APPL. MATH.
Vol. 68, No. 3, pp. 738–759

STABILITY OF TRAFFIC FLOW BEHAVIOR WITH DISTRIBUTED DELAYS MODELING THE MEMORY EFFECTS OF THE DRIVERS*

RIFAT SIPAHI†, FATIHCAN M. ATAY‡, AND SILVIU-IULIAN NICULESCU§

Abstract. Stability analysis of a single-lane microscopic car-following model is studied analytically from the perspective of delayed reactions of human drivers. In the literature, the delayed reactions of the drivers are modeled with discrete delays, which assume that drivers make their control decisions based on the stimuli they receive from a point of time in the history. We improve this model by introducing a distribution of delays, which assumes that the control actions are based on information distributed over an interval of time in history. Such an assumption is more realistic, as it takes into consideration the memory capabilities of the drivers and the inevitable heterogeneity of their delay times. We calculate exact stability regions in the parameter space of some realistic delay distributions. Case studies are provided demonstrating the application of the results.

Key words. memory, distributed delay, traffic dynamics, traffic flow stability

AMS subject classifications. 34K20, 34K60, 93D20

DOI. 10.1137/060673813

1. Introduction.

Traffic behavior has been an important research topic since the 1930s, with the of aim of reducing the undesirable social (e.g., vehicle accidents) and economic (for example, congestion and increasing pollution) effects of increasingly complex traffic loads. For this purpose, one needs a good understanding of traffic dynamics, in which many parameters or constraints play an important role, such as the physical conditions of highways, mechanical properties of vehicles, psychological states of the drivers, traffic laws, on- and off-ramps, multiple lanes, traffic density, etc. The literature contains various models addressing different phenomena; see, e.g., the survey [12] and the references therein.

Among the parameters that play a major role in traffic behavior, there exists a critical one which has been recognized as early as the 1950s [4], namely the *time delay*. It mainly originates due to the time needed by human drivers for sensing, being conscious, and performing control actions [7]. Consequently, traffic dynamics, and ultimately its mathematical models, *inherently* carry *time delays*. See, e.g., [2, 23, 19, 18, 26, 27] for some delay models and related discussions.

Stability characterizations of traffic models may be quite different when time delays are taken into account; for instance, a stable delay-free dynamics may become unstable when delays are considered. Therefore, a thorough stability analysis of the dynamics in the time delay domain is necessary. Without entering into details, we shall consider a continuous-time microscopic car-following model proposed in [4, 21] to describe traffic behavior. What distinguishes this study is the idea of incorporating *distributed delays* in order to represent the memory of the drivers.

*Received by the editors October 31, 2006; accepted for publication (in revised form) September 19, 2007; published electronically December 20, 2007.
http://www.siam.org/journals/siap/68-3/67381.html
†Corresponding author. Department of Mechanical and Industrial Engineering, Northeastern University, Boston, MA 02115 (rifat@coe.neu.edu).
‡Max Planck Institute for Mathematics in the Sciences, Inselstr. 22, Leipzig 04103, Germany (atay@member.ams.org).
§Laboratoire de Signaux et Systèmes (L2S), Supélec, 3, rue Joliot Curie, 91190, Gif-sur-Yvette, France (Silviu.Niculescu@lss.supelec.fr).

Human-in-the-loop modeling. From the perspective of control theory, traffic flow can be seen as human-in-the-loop dynamics [16], since human drivers play the major role in the evolution of the traffic flow. Such a dynamical structure exhibits richer and more complicated features not only due to the challenges of modeling human beings, but also due to the delayed control actions of the drivers, which distinguishes them from fast response characteristics of sensors and controllers. On the other hand, *the modeling of time-delays* representing the behavior of the drivers is a challenge. Models in the existing literature make use of discrete delays [2, 27, 23], which describe an action of the driver at time t that is based on what is experienced at a point of time $t - \tau$, $\tau \geq 0$, in the past. The stability of the arising dynamics has been studied by several authors from various perspectives. See [2, 6, 18, 19] for the utilization of nonlinear optimal velocity functions relating headway versus desired velocity; [19, 18, 20] for one- and two dimensional bifurcation analysis as well as phase diagrams characterizing oscillations, collision, and the stopping motion nature of the traffic flow; [27] for incorporating human driver modeling into traffic flow where human adaptation and anticipation are considered along with multiple vehicle following strategies and phase diagrams revealing collisions, oscillations, and accident-free traffic flow; and [23] for the stability analysis of traffic flow in which multiple discrete time-delays corresponding to different time scales of reaction of human drivers against velocity and headway changes are taken into account.

We note, however, that discrete-delay models can have their shortcomings. For instance, regarding τ as a fixed unchanging quantity with known value would ignore the possibility that the dynamics may possess inherent "memory" effects which use the past history of the received information. Especially for the traffic flow, the presence of human drivers suggests that memory effects should be taken into consideration. Moreover, the behavior of individual drivers and their reactions are not identical, and in reality exhibit a distribution of inhomogeneous behavior. Therefore, the use of a model taking into account the distributed nature of the delays will yield a better representation of reality. Such an argument has also some potential in modeling the dynamics of human-in-the-loop systems [16], which will ultimately open new research directions for designing driver assistance or semiactive controllers that can guide the human beings for a safer drive in uncertain environments.

In the present work, motivated by the above reasoning, we model the delayed action/decision of human drivers using distributed delays. The physical basis of the model is the fact that the drivers perform their decisions based on what they continuously observe (during a memory window) from the evolving traffic flow, during which some information is retained and used in the decision-making process. These decisions are clearly limited by the capacity of the memory, i.e., the size of the memory window, which will be an important parameter in the analysis.

Objective and approach. The main objectives of the paper are to (a) study the stability margin of the traffic flow dynamics over a microscopic car-following model in the parameter space defining the memory effects, and (b) discuss the analytical and physical interpretations of the results for several practical traffic scenarios.

For the stability analysis, we use a frequency-domain approach combined with some simple geometric ideas, and give necessary and sufficient conditions for the stability of the dynamics. In this context, we also explore whether the stability region consists of a single connected set or of several "islands" (also called *pockets*) of stability. We note that in the present text the stability is robust against small delay variations (section 2); thus small delay perturbations do not induce instability; see

some discussions in [24, 10, 17, 15]. The focus of the work here is an analytical study of the effects of distributed delays on the stability of traffic flow.

Moreover, it is shown in [1] that distributed memory enhances the stability margin in a network stabilization scheme. It is interesting to see whether a similar stability-enhancing feature also exists in traffic flow dynamics when the drivers make use of the past history of the traffic evolution in their decision-making, which would clearly have significance in realistic traffic modeling.

To model memory effects one can use common delay distributions, namely γ-distribution with and without a gap, uniform distribution. As discussed below, the first two cases are easier to handle, whereas the uniform distribution needs a more careful treatment. This mainly originates from a characteristic equation which does not exactly fit into standard classes treated in the literature, in that (i) the delay terms appear not only in exponential terms but also in the coefficients, (ii) the characteristic equation includes complex coefficients, which does not carry the features of those with real coefficients as treated in the literature [24, 17, 10, 15], (iii) there exist two independent delay parameters; stability investigations under the presence of more than one delay is quite complicated [9, 17, 22, 25, 24, 15].

The key ideas of our analysis are based on decoupling the dynamics into lower dimensions and introducing an interconnection scheme interpretation from control feedback systems theory. Such an analysis is the key to the complete analytical treatment of the arising characteristic equation. Connections with existing approaches and methodologies will be made in the following sections. In section 2, we present the microscopic car-following model and the spatial configuration of vehicles in traffic. Section 3 introduces some preliminaries, and section 4 is devoted to the main results on the stability analysis, where analytical and geometrical arguments for deriving the stability results are developed. Section 5 illustrates the results with numerical examples for several traffic scenarios, and a brief summary in section 6 concludes the presentation.

Notation. We use $\mathbb{R}$ for real numbers, where an additional $+$ or $-$ sign as a subscript indicates the positive and negative real numbers, respectively. Similarly, $\mathbb{C}_+$ and $\mathbb{C}_-$ denote complex numbers with positive and negative real parts, respectively. The imaginary axis of the complex plane is denoted by $j\mathbb{R}$, where $j = \sqrt{-1}$. We use $s \in \mathbb{C}$ for the Laplace variable, whose values on the imaginary axis are denoted by $s = j\omega$ for $\omega \in \mathbb{R}$. The eigenvalues of the matrix A are represented by $\lambda_i(A)$. $\angle z$ denotes the argument of the complex number z.

2. Microscopic car-following model with distributed delays. Although undesirable, the presence of time-delays in the process of decision making and performing a control action by human drivers is neither avoidable nor negligible (e.g., [27, 26, 2, 23]). In this section, we develop memory effects on a conceptual microscopic car-following model.

Microscopic car-following model. In order to understand the behavior of traffic flow and to propose ways to avoid its undesirable effects (congestion, accidents, economic losses, time losses, degradation of the quality of the environment), various mathematical models have been proposed in the literature [8, 12, 6, 18, 27, 26]. Despite the available results, the topic still offers open problems today.

A main direction in traffic research is focused on highway traffic models [27, 19, 12, 6], since travel times on highways are longer and travel speed is relatively high, and health and economic issues are largely at risk [12]. Furthermore, in most cases a single-lane problem is considered. Such an assumption is quite realistic and also

allows one to obtain further insight on the problem due to its simpler mathematical formulation. This type of model also forms the main focus in our study. A single-lane traffic flow, in which a chain of vehicles travels at a constant velocity (so-called quasi steady-state) without changing lanes, is considered. We use a *microscopic model* in which the dynamics of individual vehicles and drivers is taken into account. Despite the simplicity of the model, an *analytical* stability investigation becomes nontrivial due to the presence of time-delays, as we present below. Furthermore, there exist various complications in realistically modeling human beings and their delayed reactions.

The primary interest in this work is to shed light, from the perspective of memory effects of human drivers, on the stability of traffic behavior. As a starting point in this new direction, the linear stability analysis of the perturbations around the constant-velocity solutions will be of particular interest in order to reveal the stability features with respect to the parametric domain defining the memory effects. In order to achieve this, a linear mathematical model inspired by earlier work is introduced in what follows. Due to the linear stability analysis, however, the mathematical model considered here is not dependent on some additional parameters defining the traffic, such as dependence on headway, drivers' sensitivity as a function of headway, acceleration and deceleration characteristics, human anticipation, etc. Readers are directed to the work in [6, 12, 20, 27] for more elaborate models.

Discrete-delay models. Many studies in the literature model the time-delayed actions of the drivers by a discrete delay τ. One such microscopic car-following model is given as [4, 12, 21, 23]

$$\dot{v}_i(t) = \kappa_i(v_{i-1}(t-\tau) - v_i(t-\tau)). \tag{2.1}$$

This model represents the dynamics of the velocity perturbations v_i around constant-velocity solutions (the equilibrium at which *all* vehicles travel at a constant velocity V) of the traffic flow. The parameter $\kappa_i > 0$ denotes the sensitivity of a driver to the velocity difference between his vehicle and the one in front, and gives a measure of the driver's reactivity (aggressiveness) based on his experience and knowledge of the environment. For further information on discrete-delay models, refer to [2, 6, 18, 20, 27]; on the links between the stability features of discrete-delay models and Hopf bifurcations, some interesting arguments can be found in [18, 20, 19]; and on the phase diagrams of traffic flow characterizing collisions, oscillations, and accident-free flow, see [20, 27]. The cited references are also valuable sources for various mathematical models over which additional parameters not considered here, such as headway, sensitivity, acceleration, and deceleration dependence can be studied.

Distributed delay model. By incorporating a general memory effect, $f(\tau)$, into the system (2.1), we arrive at the following generalized model:

$$\dot{v}_i(t) = \kappa_i \int_0^\infty f(\tau)(v_{i-1}(t-\tau) - v_i(t-\tau))\, d\tau, \tag{2.2}$$

where we assume that the delay kernel f is a measurable function of exponential order. When f is a Dirac delta function, (2.2) reduces to the discrete delay model (2.1). See above for discussions of earlier work on discrete delay models.

Delay distributions. We will consider the following common distribution functions f in the model (2.2):

(1) *Uniform distribution.* For $\delta > 0$ and $h \geq 0$, the distribution

$$f(\tau) = \begin{cases} 1/\delta & \text{if } h < \tau < h + \delta, \\ 0 & \text{otherwise,} \end{cases} \tag{2.3}$$

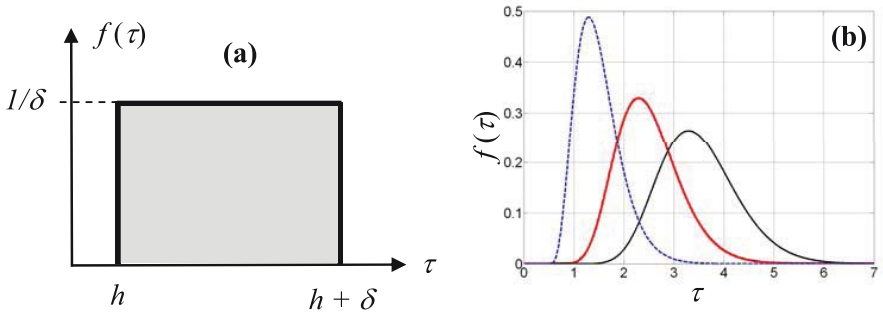

FIG. 2.1. (a) *Uniform distribution with h being dead-time and δ being size of the memory window.* (b) *γ-distribution with gap, $h = 0.5$, for $p = 5$ (dashed curve), $p = 10$ (thick curve), $p = 20$ (thin curve), where $pq = 1$.*

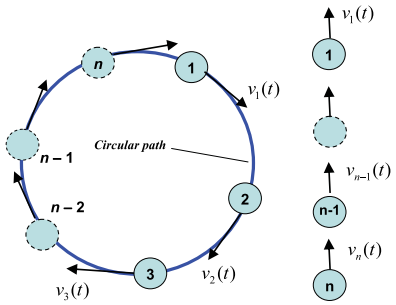

FIG. 2.2. *Ring and linear configurations of the traffic model with n vehicles.*

represents an average of the information available in the short-term memory, and can be considered as a first order approximation to a more complicated distribution; see Figure 2.1(a). It will be of interest to see how h (corresponding to some dead-time before the perception of the sensory input by the driver) and the window size δ affect the stability.

(2) *γ-distribution with and without gap.* We have

$$f(\tau) = \begin{cases} \dfrac{(\tau - h)^{p-1} e^{-(\tau-h)/q}}{q^p \Gamma(p)} & \text{if } \tau \geq h, \\ 0 & \text{if } \tau < h, \end{cases} \tag{2.4}$$

where p, q are positive parameters of the distribution, Γ denotes the gamma function, and the gap $h \geq 0$ represents the dead-time. The mean value of f is $h + pq$, and the variance is pq^2 (which exist for $p > 2$), which is a measure of the length of the memory window, q being a scaling factor ($q = 1$, mean value $= h + p$, variance $= p$). It will be of interest to see how the quantities h, p, and q affect stability. See in Figure 2.1(b) the γ-distribution with gap for various p values keeping pq fixed.

Spatial configuration of the model. We consider two widely utilized configurations (Figure 2.2) with n number of vehicles: (a) vehicles traveling around a ring, and (b) vehicles arranged along a linear path. In the linear configuration, the vehicle in front (for which we use the convention of labeling with index $i = 1$) travels at a constant velocity, i.e., $\dot{v}_1(t) = 0$. Hence, the linear configuration can be derived from the circular one by setting $\kappa_1 = 0$.

3. Problem statement and preliminaries. The system (2.2) can be expressed in vector form as

$$\dot{\mathbf{v}}(t) = \int_0^\infty J\mathbf{v}(t-\tau)f(\tau)\,d\tau, \tag{3.1}$$

where $\mathbf{v} = (v_1, \ldots, v_n)$ and $J \in \mathbf{R}^{n\times n}$ is a configuration matrix weighted by the driver sensitivities κ_i. For the *circular* form of the configuration in Figure 2.2, it is obvious that $v_0 = v_n$; thus the appropriate index selection in (2.2) becomes $i = 1, \ldots, n$. Consequently, the matrix J takes the form

$$J = \begin{pmatrix} -\kappa_1 & 0 & \cdots & 0 & \kappa_1 \\ \kappa_2 & -\kappa_2 & 0 & \cdots & 0 \\ 0 & \kappa_3 & -\kappa_3 & \cdots & 0 \\ \vdots & \vdots & \ddots & \ddots & \vdots \\ 0 & \cdots & 0 & \kappa_n & -\kappa_n \end{pmatrix}. \tag{3.2}$$

The configuration matrix for the linear arrangement of vehicles is obtained by setting $\kappa_1 = 0$, and it is denoted by J'.

The characteristic equation for (3.1) is given by

$$\chi(s) = \det[sI - JF(s)] = 0, \tag{3.3}$$

where $F(s)$ is the Laplace transform of f. We assume the generic case that J is diagonalizable; that is, its eigenvectors form a basis for $\mathbb{R}^n$. Then (3.3) can be expressed as $\chi(s) = \prod_{i=1}^n (s - \lambda_i(J)F(s)) = 0$, where $\lambda_i(J)$ is the ith eigenvalue of J. In the remainder of the text, λ_i will denote $\lambda_i(J)$ unless otherwise stated. The roots corresponding to the ith factor of χ, i.e., the solutions s of the equation

$$\chi_i(s) \triangleq s - \lambda_i F(s) = 0, \tag{3.4}$$

determine the fate of perturbations along the ith eigenvector of J. The perturbations die out if and only if $\mathrm{Re(s)} < 0$ for all solutions s of (3.4). As the stability depends on the spectrum of J, the following properties will be needed in the analysis.

LEMMA 3.1. *The configuration matrix J has a simple zero eigenvalue, and all its remaining eigenvalues have negative real parts. Furthermore, $|\lambda_i| \le 2\kappa_{\max}$, $i = 1, \ldots, n$, where $\kappa_{\max} = \max\{\kappa_i\}$. If $\kappa_i = \kappa$ for all i, then the eigenvalues of J are given by*

$$\lambda_i = \kappa(e^{j2\pi(i-1)/n} - 1), \qquad i = 1, \ldots, n. \tag{3.5}$$

If J' denotes the matrix obtained from J by setting $\kappa_1 = 0$, then the eigenvalues of J' are real and given by $0, -\kappa_2, -\kappa_3, \ldots, -\kappa_n$.

Proof. The rows of J sum to zero, implying that zero is an eigenvalue corresponding to the eigenvector $(1, 1, \ldots, 1)^\top$. The circular configuration corresponds to a (weighted) directed graph which is strongly connected; that is, there is a directed path from every vertex to any other vertex. It follows that zero is a simple eigenvalue of the graph Laplacian matrix, which is equal to J in the present case. Furthermore, by Gershgorin's theorem [13], the eigenvalues of J are located in the union of discs

$$\lambda_i \in \bigcup_{\ell=1}^n \mathcal{B}(-\kappa_\ell) = \mathcal{B}(-\kappa_{\max}), \tag{3.6}$$

where $\mathcal{B}(r) = \{s \in \mathbb{C} : |s - r| \leq |r|\}$ is the disc centered at $r \in \mathbb{R}$ with radius $|r|$. Hence, all nonzero eigenvalues of J have negative real parts since $\kappa_i > 0$ for all i. Moreover, $|\lambda_i| \leq 2\kappa_{\max}$ by (3.6). One can also directly calculate the characteristic polynomial of J by an easy expansion by cofactors to obtain

$$\prod_{i=1}^{n}(\lambda + \kappa_i) - \prod_{i=1}^{n}\kappa_i = 0. \tag{3.7}$$

So, if $\kappa_i = \kappa$ for all i, then $(\lambda/\kappa + 1)^n = 1$; i.e., $\lambda/\kappa + 1$ are the nth roots of unity, which yields (3.5). The spectrum of J' follows from (3.7) by setting $\kappa_1 = 0$. ∎

We make the convention of labeling the zero eigenvalue of J as λ_1, and denote the corresponding eigenvector as $v_1 = (1, 1, \ldots, 1)^\top$. Hence, $\mathrm{Re}(\lambda_i) < 0$ for $i \geq 2$. Note that $s = 0$ is a solution of (3.4) when $i = 1$. This is the indicator of the rigid body rotation of the whole configuration of vehicles, and consequently the stability of the configuration is determined by the roots of the modified characteristic equation

$$\hat{\chi}(s) = \prod_{i=2}^{n}(s - \lambda_i F(s)) = 0. \tag{3.8}$$

Hence, car-following dynamics given by (2.2) is stable if all solutions s of (3.8) have negative real parts.

REMARK 3.2. *Notice that all roots of the delay-free form of* (3.8) *are stable, as per Lemma* 3.1. *This forms only the starting point of the stability analysis. The main results presented in the following section reveal the necessary and sufficient conditions for the complete stability analysis of* (2.2) *with respect to the parametric domain of interest: delay distribution $f(\tau)$ and the spectrum of J. Readers are directed to some other models in the earlier cited references for the incorporation of additional parameters that may play a role in the stability of traffic dynamics.*

4. Main results. We first introduce an interconnection scheme idea for the characteristic equation (3.8), which will allow a geometric approach to the stability analysis by an appropriate separation of parameters.

4.1. Interconnection scheme interpretation. Consider first the uniform distribution (2.3), whose Laplace transform is

$$F(s) = \frac{e^{-sh}(1 - e^{-s\delta})}{s\delta}. \tag{4.1}$$

Note that $F(s) \to e^{-sh}$ as $\delta \to 0$, corresponding to the fact that f approaches a Dirac delta at h, where one recovers the discrete-delay model (2.1) with $\tau = h$. Using (4.1) in (3.4) gives

$$\chi_i(s) = s - \lambda_i e^{-sh}\frac{1 - e^{-s\delta}}{s\delta} = 0. \tag{4.2}$$

The singularity of χ_i at zero is removable since $\lim_{s\to 0}\chi_i(s) = -\lambda_i$. Hence by defining $\chi_i(0) = -\lambda_i$, we can treat χ_i as an analytical function and use arguments based on the continuous dependence of its roots on the parameters. In particular, since $\lambda_i \neq 0$ for $i \geq 2$, by Lemma 3.1, the following result is immediate.

LEMMA 4.1. *$s = 0$ is not a solution to* (4.2) *for $i = 2, \ldots, n$.*

We rearrange (4.2) as

$$H_i(s) \cdot \Delta(s) = 1, \quad i = 2, \ldots, n, \tag{4.3}$$

$$\text{where} \quad H_i(s) = \frac{\lambda_i e^{-sh}}{s}, \qquad \Delta(s) = \frac{1 - e^{-s\delta}}{s\delta}. \tag{4.4}$$

The advantage of the form (4.3) lies mainly in the separation of the parameter δ and the eigenvalues of J, which will simplify the analysis. Similarly, for the γ-distribution we have $F(s) = e^{-hs}(qs+1)^{-p}$, and the corresponding characteristic equation can be expressed as an interconnection scheme,

$$H_i(s) \cdot \Delta_\gamma(s) = \frac{\lambda_i e^{-sh}}{s} \cdot \frac{1}{(qs+1)^p} = 1. \tag{4.5}$$

Note that $|\Delta_\gamma(j\omega)| \leq 1 \ \forall \omega \in \mathbf{R}$, for any q.

4.2. Stability analysis. Given λ_i, the roots of (3.8) depend continuously on the parameters of the distribution $f(\tau)$ (see [5]). The method for stability analysis can then be summarized as follows. (a) Check the stability of the delay-free dynamics (3.8). (b) Calculate the characteristic roots on the imaginary axis, $s = j\omega$, of the interconnection scheme $H_i(s)\Delta(s) - 1 = 0$. (c) Check in which direction $s = j\omega$ crosses the imaginary axis with respect to the parametric domain of interest. Notice that the characteristic equation in (4.2) does not necessarily exhibit complex conjugate s solutions if $\lambda_i \in \mathbb{C}$.

We present below the stability analysis of (4.3) for the case of uniform distribution. The technique is easily extendable to γ-distribution with and without a gap with the construct of the interconnection scheme. The challenges in assessing the stability are (i) analysis should be performed in the multiple parameter space (h, δ, λ_i); (ii) the interconnection scheme carries complex coefficients; (iii) one of the parameters from (i), δ, appears both in an exponent and in the denominator of the interconnection scheme. The complications (i)–(iii) prevent our benefiting from many stability analysis techniques [3, 24, 17, 22, 15]. Before we introduce how to tackle these difficulties, we start with some conditions for the roots of (4.3) to exhibit imaginary axis crossings.

The following algorithm enables the calculation of the curves in the (h, δ) domain on which (4.3) has a solution of the form $s = j\omega$.

COMPUTATION ALGORITHM FOR $s = j\omega$ AND (h, δ) PAIRS. Given λ_i, the characteristic roots $s = j\omega$ crossing the imaginary axis and the corresponding parameter pairs (h, δ) can be exhaustively computed as follows. First, we write the magnitude condition in (4.3), at $s = j\omega$, which allows us to compute δ independently from h. (This is a direct consequence of the separation feature introduced by the interconnection scheme interpretation.) Second, on the same equation (4.2), we write the argument condition, which yields h.

Step 1. Define the continuous function $f_\Delta : \mathbb{R} \to \mathbb{R}_+$ by

$$f_\Delta(u) = \begin{cases} \sin^2 u/u^2, & u \neq 0, \\ 1, & u = 0. \end{cases} \tag{4.6}$$

Let

$$u = \frac{\delta\omega}{2} \in \mathbb{R}. \tag{4.7}$$

Step 2. By substituting (4.7) into the magnitude of (4.3),

$$|H_i(j\omega)|^2|\Delta(j\omega)|^2 = 1, \tag{4.8}$$

one obtains

$$\frac{|\lambda_i|^2}{(\omega)^2} f_\Delta(u) = 1, \tag{4.9}$$

which can be alternatively written as

$$f_\Delta(u)\frac{|\lambda_i|^2\delta^2}{4u^2} = 1 \Rightarrow f_\Delta(u) = \frac{4u^2}{|\lambda_i|^2\delta^2} = ku^2, \tag{4.10}$$

where $k = 4/(|\lambda_i|^2\delta^2)$.

The following proposition is immediate using Steps 1–2 above.

PROPOSITION 4.2 (frequency-sweeping characterization [17]). *$s = j\omega$ is a root of (4.3) if and only if $\omega \leq |\lambda_i|$.*

Proof. It is clear from (4.6) and (4.7) that $|H_i(j\omega)| = |\lambda_i|/|\omega| > 1$ should be satisfied such that (4.8) holds. ∎

Step 3. One simply *sweeps* u and obtains ω from (4.9).

Step 4. Using u and ω from Step 3, solve for δ from (4.7).

Step 5. Define next

$$\lambda_i = |\lambda_i|e^{j\phi_i} \quad \text{with } \phi_i = \angle\lambda_i, \tag{4.11}$$

where $\phi \in (\pi/2, 3\pi/2)$ as per Lemma 3.1, and use the argument condition on (4.3) to compute h.

Step 6. Rearrange (4.3) as

$$e^{-j\omega h} = \frac{-\delta(\omega)^2}{\lambda_i(1 - e^{-j\delta\omega})},$$

from which one obtains the following by equating the arguments of both sides:

$$h = \frac{1}{\omega}[-\pi + \phi_i + \angle(1 - \cos(\delta\omega) + j\sin(\delta\omega)) + 2\pi\ell], \quad \ell \in \mathbb{Z}. \tag{4.12}$$

Step 7. Using (4.7), it is clear that $\angle(1 - \cos(\delta\omega) + j\sin(\delta\omega)) = \tan^{-1}\left(\frac{\cos u}{\sin u}\right) = \frac{\pi}{2} - u$, simplifying (4.12) to

$$h = \frac{1}{\omega}\left(-\frac{\pi}{2} + \phi_i - u + 2\pi\ell\right). \tag{4.13}$$

PROPOSITION 4.3. *There exists a connected stability region of the traffic flow dynamics (2.2) in the parameter space (h, δ) that includes the origin $(h, \delta) = (0, 0)$. The bounds of this region on the δ and h axes are respectively given by*

$$\bar{h} = \min_{2\leq i\leq n}\left(\frac{2\phi_i - \pi}{2|\lambda_i|}\right) \quad \textit{and} \quad \bar{\delta} = \min_{2\leq i\leq n}\left(-\frac{(2\phi_i - \pi)^2}{2|\lambda_i|\cos(\phi_i)}\right). \tag{4.14}$$

REMARK 4.4. *We shall show later that the stability region mentioned in the above proposition is actually the unique stability region in the parameter space.*

Proof. When $h = \delta = 0$, the distribution function in (2.3) is a Dirac delta whose Laplace transform equals 1. From (4.2), the characteristic roots are $s = \lambda_i$, $i = 2, \ldots, n$, where $\mathrm{Re}(\lambda_i) < 0$ by Lemma 3.1. Thus, (2.2) is stable for $(h, \delta) = (0, 0)$. Consequently, the stability region in the (h, δ) parameter domain contains an open neighborhood of the origin $(h, \delta) = (0, 0)$ [5]. We next calculate the stability margins along the δ- and h-axes.

Stability when $\delta = 0$. For $\delta \to 0$ the characteristic equation (4.2) becomes

$$s = \lambda_i e^{-sh}. \tag{4.15}$$

Equation (4.15) has a stable root for $h = 0$ (see Proposition 4.3), and stability is lost if a characteristic root crosses the imaginary axis for some $h \neq 0$. Thus, the stability is preserved between $h = 0$ and the minimum positive h for which (4.15) has a solution $s = j\omega$. This minimum h is computed as follows. By Lemma 4.1, the magnitude condition on (4.15) yields $\omega = \mp|\lambda_i|$, and the argument condition requires

$$h = \frac{1}{|\lambda_i|}\left(-\frac{\pi}{2} \mp \phi_i + 2\pi\ell\right), \quad \ell \in \mathbb{Z}, \tag{4.16}$$

with $+\phi_i$ when $\omega > 0$. Using the above equation, one obtains the smallest positive h, $\bar{h}$ as given in (4.14). Hence, when $\delta = 0$, (4.2) is stable for $h \in [0, \bar{h})$.

Stability when $h = 0$. The smallest positive value of δ for which stability is lost is denoted by $\bar{\delta}$; that is, the stability interval along δ-axis is $\delta \in [0, \bar{\delta})$. The characteristic equation (4.2) when $h = 0$ is

$$\frac{\delta s^2}{\lambda_i} + e^{-s\delta} - 1 = 0. \tag{4.17}$$

Letting $s = j\omega$, solving for the exponential term, and equating the magnitude conditions of both sides, one easily obtains δ:

$$\delta = -\frac{2|\lambda_i|\cos(\phi_i)}{\omega^2}. \tag{4.18}$$

Moreover, solving the exponential term in (4.17), equating the arguments of both sides, substituting δ from (4.18), and noting that $\omega \neq 0$ by Lemma 4.1, we obtain

$$\omega = \frac{2|\lambda_i|\cos(\phi_i)}{\angle(-\cos(2\phi_i) + j\sin(2\phi_i)) \pm 2\pi\ell}, \quad \ell = 0, 1, 2, \ldots,$$

which simplifies and gives rise to δ

$$\omega = \frac{2|\lambda_i|\cos(\phi_i)}{\pi - 2\phi_i \mp 2\pi\ell}, \quad \delta = -\frac{(\pi - 2\phi_i \mp 2\pi\ell)^2}{2|\lambda_i|\cos(\phi_i)}. \tag{4.19}$$

When $\delta = 0$ the dynamics is stable. Following the root continuity arguments [5], the stability is lost for the smallest positive δ, which is attained when $\ell = 0$ and equal to $\bar{\delta}$ as given in (4.14). ∎

Characterization of the geometry of the stability boundaries. The stability boundaries are among those curves in the (h, δ) parametric domain which give rise to an $s = j\omega$ solution in the interconnection scheme. In order to characterize the geometry of the stability boundaries, one has to establish the link from u domain

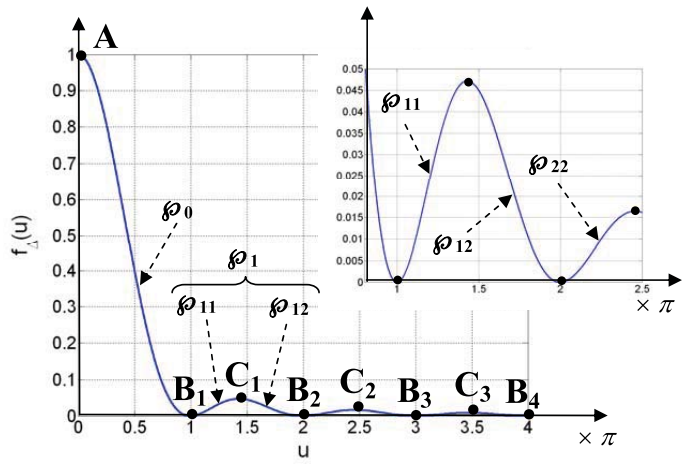

FIG. 4.1. *$f_\Delta(u)$ versus u. B_ℓ and C_ℓ are end points and the local maxima of the segments $\wp_\ell$, $\ell > 0$, respectively.*

to (h, δ). To achieve this, we give some definitions first. Define the extrema points of f_Δ function with $A(f_\Delta(0))$, $B_\ell(f_\Delta(\ell\pi))$, and $C_\ell(f_\Delta((2\ell+1)\pi/2))$, $\ell = 1, 2, 3, \ldots$; see Figure 4.1. Partition $f_\Delta(u)$ into segments and label each one of them as follows: $\wp_0 = f_\Delta(u)$ with $u \in [0, \pi]$; $\wp_{\ell,\ell} = f_\Delta(u)$ with $u \in [\ell\pi, (2\ell+1)\pi/2]$; $\wp_{\ell,\ell+1} = f_\Delta(u)$ with $u \in [(2\ell+1)\pi/2, 2\ell\pi]$, $\ell = 1, 2, 3, \ldots$. Obviously,

$$f_\Delta = \bigcup_{\ell \geq 0} \wp_\ell, \quad \text{where } \wp_\ell = \wp_{\ell,\ell} \bigcup \wp_{\ell,\ell+1} \quad \forall \ell > 0. \tag{4.20}$$

Notice that each of the "segments" $\wp_0$, $\wp_{\ell,\ell}$, and $\wp_{\ell,\ell+1}$ as a function is monotonic with respect to the variable u, as seen in Figure 4.1. The points B_ℓ and C_ℓ in this figure correspond to the end points and the local maxima of the segments $\wp_\ell$, $\ell > 0$, respectively. Due to the symmetry of the function f_Δ, $f(u) = f(-u)$, and by (4.7), we will restrict our subsequent analysis to positive ω, $\omega > 0$.

Monotonicity properties. We will now utilize the monotonicity properties of the "segments" of $f_\Delta(u)$ in order to explain how their mapping in (h, δ) forms. We first comment on the extremities in u and (h, δ) domains. Given λ_i, at point A we have $f_\Delta(u = 0) = 1$; hence from (4.8), $\omega = |\lambda_i|$ and from (4.7), $\delta = 0$. At the end points of $\wp_\ell$, that is B_ℓ and $B_{\ell+1}$, we have $\lim_{u \to \ell\pi} f_\Delta(u) \to 0^+$; thus for a solution of the interconnection scheme in the form of $s = j\omega$ to exist, it is clear from (4.9) that $\omega \to 0^+$. Therefore, the image of B_ℓ and $B_{\ell+1}$ on (h, δ) space corresponds to infinity, since these curves are open-ended curves.

Recall that if $s = j\omega$ solution of the interconnection scheme exists, then (4.10) holds. This indicates that u solutions of (4.8) lie at the intersection points of the curve $f_\Delta(u)$ and the parabola u^2 parameterized by k. This relationship is generically depicted in Figure 4.2(a) for various k values and for positive $u > 0$. Notice from (4.10) that δ is inversely proportional to k.

Let us now elaborate on Figure 4.2(a), since it depicts the geometry of the solution points in u (such as points C, D, E, and F), which we will use for characterizing the corresponding geometry in the (h, δ) domain. Denote this correspondence from u domain to (h, δ) domain by $f_\Delta(u) \mapsto \zeta(h, \delta) : \mathbb{R}_+ \mapsto \mathbb{R} \times \mathbb{R}_+$. Next, define ζ_0, $\zeta_{\ell,\ell}$,

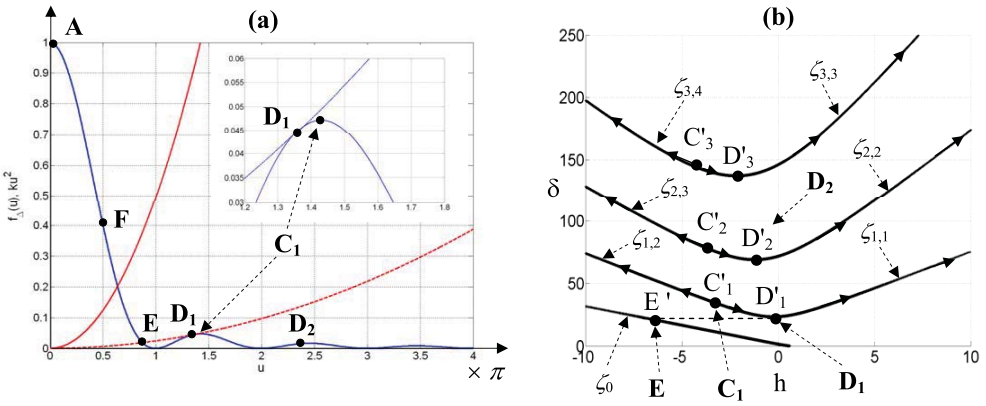

FIG. 4.2. (a) *Generic depiction of f_Δ and ku^2 versus u, where the parabola sweeps the first quadrant counterclockwise with increasing k. Inset: Distinction between points D_1 and C_1.* (b) *The mapping of the intersection points between f_Δ and ku^2 to the (h,δ) domain ($C_i \mapsto C_i'$, $D_i \mapsto D_i'$, $E \mapsto E'$, etc.). Arrows indicate decreasing direction of ω.*

and $\zeta_{\ell,\ell+1}$ segments in the (h,δ) domain that correspond to the segments $\wp_0$, $\wp_{\ell,\ell}$, and $\wp_{\ell,\ell+1}$, respectively, in u domain, and similarly, let $\zeta_\ell = \zeta_{\ell,\ell} \bigcup \zeta_{\ell,\ell+1}$ $\forall \ell > 0$. Figure 4.2(b) presents generically some of these curves in the (h,δ) domain, where E' corresponds to E of Figure 4.2(a); D_1', D_2', D_3', etc., are the mappings of the points at which the parabola in Figure 4.2(a) is tangent to $\wp_{11}$, $\wp_{22}$, $\wp_{33}$, etc., segments (shown in Figure 4.1), respectively; C_1', C_2', C_3', etc., are the mappings of the local maxima points C_1', C_2', C_3', etc., at which the maximum omega on a respective ζ_ℓ, $\ell > 0$, curve. The points C_ℓ can also be seen as the end points of $\zeta_{\ell,\ell}$ and $\zeta_{\ell,\ell+1}$ curves.

Notice that, for a given λ_i, intersection points in Figure 4.2(a) for fixed k give rise to fixed δ, as per (4.10). For instance, for a particular selection of k, the parabola may intersect $\wp_{1,1}$ and $\wp_{1,2}$, giving rise to two points, one on $\zeta_{1,1}$ and the other on the $\zeta_{1,2}$ curve. Furthermore, all such points are earmarked by ω. See the two points in Figure 4.3(c)–(d) labeled with ω_1 and ω_2 as an example.

REMARK 4.5. *The ζ_0 curve in Figure* 4.2(b) *is due to mapping of the $\wp_0$ segment; see also Figure* 4.3(a)–(b). *For the remaining segments, we state the following. For a given k, any two points at the intersection of the parabola and the segment $\wp_\ell$, $\ell > 0$, give rise to two points on the ζ_ℓ curve; see Figure* 4.3(c)–(d). *These two points are generated by two distinct u values, the larger of which corresponds to the larger ω as per* (4.9). *It is clear from* (4.13) *that larger u corresponds to smaller h. Consequently, the point marked by ω_1 in Figure* 4.3(c)–(d) *arises from the intersection between ku^2 and $\wp_{1,2}$; thus it lies on the $\zeta_{1,2}$ curve, and $\omega_1 > \omega_2$ holds. The arrows on ζ curves in Figure* 4.2(b) *and Figure* 4.3(c)–(d) *indicate the direction of decreasing ω on the respective curves. Finally, the point marked with C_ℓ indicates the location of maximum ω attained on the curve ζ_ℓ, $\ell > 0$, which is clearly due to the local maximum of the f_Δ curve in the interval $u \in (\pi, 2\pi)$ (maximum u thus maximum ω as per* (4.13)). *Figure* 4.3 *presents separately the way in which the first two curves ($\wp_0 \mapsto \zeta_0$ and $\wp_1 \mapsto \zeta_1$) are generated.*

PROPOSITION 4.6 (crossing curve characterization). *The boundary of the stability region defined in Proposition* 4.3 *and depicted in Figure* 4.3 *arises from the correspondence $\wp_0(u) \mapsto \zeta_0(h,\delta)$. The necessary and sufficient condition forming this boundary in the (h,δ) domain is obtained only from the interval $u \in [0, \pi/2)$.*

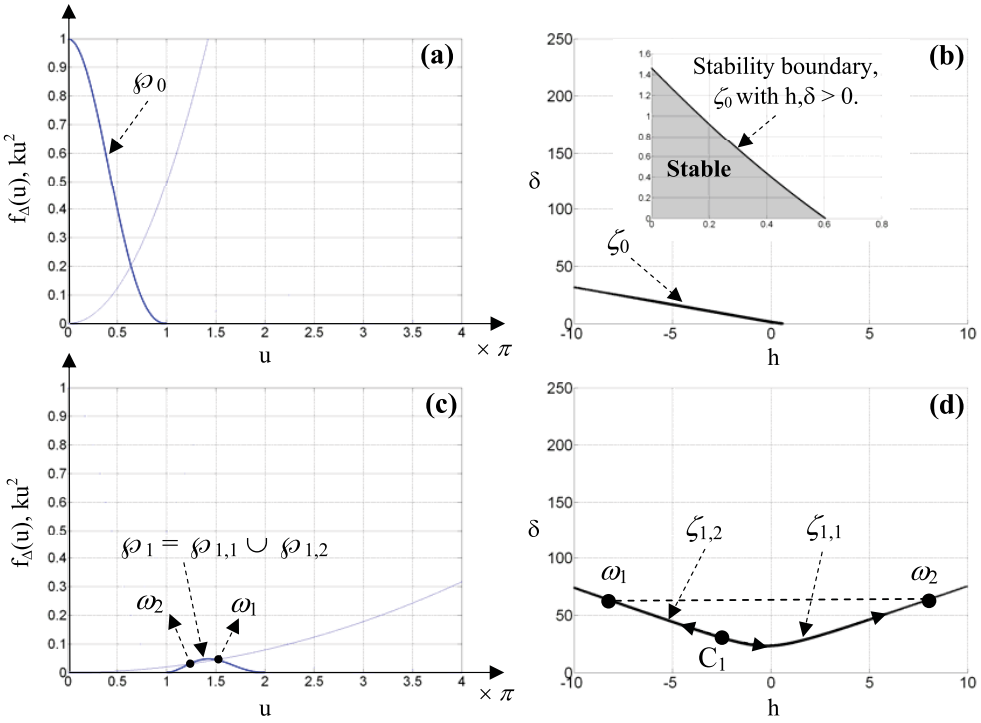

FIG. 4.3. (a)–(b) *Mapping of* $\wp_0$ *to* ζ_0. (c)–(d) *Mapping of* $\wp_1 = \wp_{1,1} \cup \wp_{1,2}$ *to* $\zeta_1 = \zeta_{1,1} \cup \zeta_{1,2}$ *(*$\wp_{1,i} \mapsto \zeta_{1,i}$*, for* $i = 1, 2$*). Arrows indicate the decreasing direction of* ω*, which attains its maximum on a respective* ζ_ℓ *curve at point* C_ℓ*,* $\ell > 0$.

Proof. (i) *Condition* $u \in [0, \pi/2)$. By Proposition 4.3, the stability boundary intersecting the h axis, $\bar{h}$, is created when $\delta = 0$. Since $\delta = 0$ corresponds to $u = 0$, starting from $u = 0$, tracing the intersection points of the parabola ku^2 and the curve $\wp_0$, one extracts the boundary of the single connected stability region in (h, δ). On this boundary, δ is monotonically increasing considering (4.7) and Proposition 4.8. To complete the proof, one should take into account the constraint of $h > 0$. Hence, δ should increase until h becomes zero. This occurs when the boundary of the stability region intersects the δ-axis at $\bar{\delta}$; see Proposition 4.3. The u value corresponding to $\bar{\delta}$ is $u = \omega\delta/2 < \pi/2$ as per (4.19).

(ii) *Necessary and sufficient condition.* There exists no u interval other than $u \in [0, \pi/2)$ that gives rise to a (h, δ) point on the stability boundary, since $f_\Delta(u)$ values attained in the interval $u \in [0, \pi/2)$ cannot be attained by any $u > \pi/2$. Hence $u \in [0, \pi/2)$ is necessary and sufficient for the computation of this boundary. ∎

REMARK 4.7. *Geometrically, the interval* $u \in [0, \pi/2)$ *corresponds to the segment AF in Figure* 4.2(a).

PROPOSITION 4.8 (local monotonicity property). *On the stability boundary, increasing* k *monotonically decreases* u *and* δ *solutions arising from the intersection points between* $f_\Delta(u)$ *and the parabola* ku^2.

Proof. From (4.10), $k = f_\Delta(u)/u^2$. The variation of k with respect to u is $\frac{dk}{du} = f'_\Delta(u)\frac{1}{u^2} - \frac{2}{u^3}f_\Delta(u)$. Since $f_\Delta(u) > 0$ and $f'_\Delta(u) < 0$ in the interval $u \in [0, \pi/2)$ defining the stability boundary, dk/du is negative. Recall that δ and k are inversely proportional; thus δ on the stability boundary is decreasing for increasing k. ∎

Readers are directed to the work in [11] as an example of the deployment of monotonicity ideas which gives rise to the characterization of the geometry of stability regions of a class of delay differential equations.

LEMMA 4.9. *dh/du on the stability boundary is nonpositive for all $u \in [0, \frac{\pi}{2})$.*

Proof. From (4.9), $\omega^2 = f_\Delta |\lambda_i|^2$. For $u \in [0, \pi/2)$, one can take $\omega = \sqrt{f_\Delta}|\lambda_i| = \sin(u)|\lambda_i|/u$ for studying the variations of h in (4.13). Note that the h variation on the stability boundary is obtained for $\ell = 0$; see Proposition 4.3. Hence, the variation of h along the stability boundary is found as

$$\frac{d}{du}\frac{(\phi_i - \pi/2 - u)u}{|\lambda_i|\sin(u)} = -\frac{A(u)\phi_i + B(u)}{2|\lambda_i|\sin^2(u)}, \tag{4.21}$$

where $A(u) = 2u\cos u - 2\sin u$ and $B(u) = 4u\sin u - u\pi\cos u - 2u^2\cos u + \pi\sin u$. Notice that $A(u) < 0$ for all $u \in (0, \pi/2)$ since $u < \tan(u)$ in this interval; thus the inequality in (4.21) becomes $A(u)\phi_i + B(u) > 0$, which can be rewritten as

$$-\frac{B(u)}{A(u)} > \phi_i \quad \forall u \in \left(0, \frac{\pi}{2}\right),$$

where in our case $\phi_i \in (\pi/2, 3\pi/2)$. Consequently, it is sufficient to prove that $-B(u)/A(u) > 3\pi/2$, that is,

$$\frac{2u - \pi}{u - \pi} - \frac{u}{\tan(u)} < 0 \quad \forall u \in \left(0, \frac{\pi}{2}\right).$$

The fact that the above inequality holds can be seen from Figure 4.4. Although an analytical proof can be given, the algebraic manipulations are rather involved and thus omitted. ∎

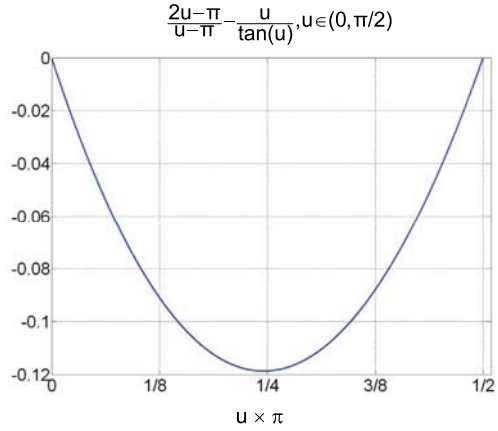

FIG. 4.4. *Plot of $\frac{2u-\pi}{u-\pi} - \frac{u}{\tan(u)}$ versus u, $u \in (0, \pi/2)$.*

REMARK 4.10. *By Proposition 4.8 and Lemma 4.9, increasing u corresponds to increasing δ and decreasing h. Hence, on the stability boundary, we have the property $\frac{\partial \delta}{\partial u}\frac{\partial u}{\partial h} = \frac{\partial \delta}{\partial h} < 0$.*

REMARK 4.11. *Since parameter u depicting the stability boundary is bounded as per Proposition 4.6, all ω satisfying the interconnection scheme belong to the set $\Gamma_\omega = \{\omega \mid H_i(j\omega)\Delta(j\omega) - 1 = 0,\ u = \delta\omega/2,\ u \in [0, \pi/2)\}$. As such, the imaginary roots on the stability boundary are given by the set $j\Gamma_\omega$. From (4.9), one can obtain*

Γ_ω *as* $\Gamma_\omega = (\sqrt{2}|\lambda_i|/\pi, |\lambda_i|]$. *This interval of* ω *is obviously a subset of the interval claimed in Proposition* 4.2*, since the interval of* u *creating the stability boundary is now restricted as* $u \in [0, \pi/2)$.

Let us comment on the remaining part of the $\wp_0$ curve, $u \in (\pi/2, \pi)$. Following part (i) of the above proof, we state that corresponding h values obtained by u, $u \in (\pi/2, \pi)$, are all negative and thus ignored. Values of h on the curves obtained by the shifting $2\pi\ell/\omega$, $\ell = 1, 2, \ldots$, as per (4.13), however, may become positive, and thus should be carefully treated.

PROPOSITION 4.12 (crossing curves property). *The curves* $\zeta_{\ell,\ell}$ *and* $\zeta_{\ell,\ell+1}$, $\ell \geq 1$, *do not intersect the stability boundary formed by* ζ_0.

Proof. It is sufficient to prove $\inf_{\delta \in (\zeta_{\ell,\ell} \cup \zeta_{\ell,\ell+1})} \delta > \sup_{\delta \in \zeta_0} \delta$. From Proposition 4.8, it is clear that $\inf_{\delta \in (\zeta_{\ell,\ell} \cup \zeta_{\ell,\ell+1})} \delta$ arises from the $u = u_1$ value at point D_1 in Figure 4.2. As per Propositions 4.6 and 4.8, $\sup_{\delta \in \zeta_0} \delta$ is found at $u = \pi/2$ (point F in Figure 4.2). Since $u_1 > \pi/2$, using Proposition 4.8, one can see that the inequality $\inf_{\delta \in (\zeta_{\ell,\ell} \cup \zeta_{\ell,\ell+1})} \delta > \sup_{\delta \in \zeta_0} \delta$ holds. ∎

It is now proven that ζ_0 does not intersect with the remaining $\zeta_{\ell,i}$ ($i = \ell, \ell+1$, $\ell \geq 1$) segments; however, one also needs to show *stability properties* around the regions bordered by all the ζ curves in order to reveal the stability regions in the parametric domain of (h, δ). The following proposition helps achieve this.

PROPOSITION 4.13 (crossing direction along h, for δ fixed). *Given* λ_i *and* δ*, the crossing direction of the imaginary root(s)* $s = j\omega$ *along the* h*-axis is independent of the delays* $h + \frac{2\pi}{\omega}\ell$, $\ell = 0, 1, \ldots$, *creating these imaginary roots.*

Proof. The characteristic equation χ_i in (4.2) can be expressed as $\chi_i = s - \lambda_i e^{-sh}\Delta(s) = 0$ using (4.4). Then, the sensitivity expression at $s = j\omega$, after suppressing the arguments to conserve space, becomes

(4.22)
$$S(j\omega) = \left.\frac{ds}{dh}\right|_{s=j\omega} = \left(-\frac{\partial \chi_i}{\partial h}\left(\frac{\partial \chi_i}{\partial s}\right)^{-1}\right)_{s=j\omega} = -\left.\frac{s\lambda_i e^{-sh}\Delta}{1 + \lambda_i e^{-sh}(h\Delta - \Delta')}\right|_{s=j\omega},$$

where $\Delta' = \frac{\partial \Delta}{\partial s}$. The above equation simplifies to

$$S(j\omega) = -\left.\frac{s\Delta}{\lambda_i^{-1}e^{sh} + h\Delta - \Delta'}\right|_{s=j\omega}. \tag{4.23}$$

Let $S(j\omega) = \frac{S_{NR}(\omega) + jS_{NI}(\omega)}{S_{DR}(\omega) + jS_{DI}(\omega)}$ with $S_{NR}, S_{NI}, S_{DR}, S_{DI} \in \mathbb{R}$. Then the real part of (4.23), which indicates the crossing direction of the $s = j\omega$ root across the imaginary axis, becomes

$$\Re\left(S(j\omega)\right) = \frac{S_{NR}S_{DR} + S_{NI}S_{DI}}{S_{DR}^2 + S_{DI}^2}. \tag{4.24}$$

Notice that if $\mathrm{sgn}(\Re\left(S(j\omega)\right)) = +1$ (or -1), this will indicate an imaginary axis crossing from left to right (or from right to left) half of the complex plane. Since the denominator of (4.24) is positive, it is dropped for studying the sign. Consequently, the numerator of (4.24) will determine the crossing direction, which becomes

$$\begin{aligned}
&\omega\left(\Im(\Delta)\left(h\Re(\Delta) - \Re(\Delta') + \Re\left(\frac{e^{jh\omega}}{\lambda_i}\right)\right) - \Re(\Delta)\left(h\Im(\Delta) - \Im(\Delta') + \Im\left(\frac{e^{jh\omega}}{\lambda_i}\right)\right)\right) \\
&= \omega\left(\Im(\Delta)\left(-\Re(\Delta') + \Re\left(\frac{e^{jh\omega}}{\lambda_i}\right)\right) - \Re(\Delta)\left(-\Im(\Delta') + \Im\left(\frac{e^{jh\omega}}{\lambda_i}\right)\right)\right).
\end{aligned} \tag{4.25}$$

After some manipulations and dropping $\omega > 0$, this yields

$$\operatorname{sgn}\left(\Re\left(S(j\omega)\right)\right) = \operatorname{sgn}\left(\Im\left(\bar{\Delta}(j\omega)(\Delta'(j\omega) - \lambda_i^{-1}e^{jh\omega})\right)\right), \tag{4.26}$$

where $\bar{\Delta}(j\omega)$ is the complex conjugate of $\Delta(j\omega)$. Notice that the above equation is independent of h due to the exponential terms $e^{jh\omega}$ remaining unchanged for the selection of $h + \frac{2\pi}{\omega}\ell$, $\ell = 0, 1, \ldots$. ∎

REMARK 4.14. *The invariance feature of the root sensitivity expression in* (4.26) *enables an effective tool which helps reveal the stability/instability regions of the traffic dynamics in the entire* $(h, \delta) \in \mathbb{R}^2_+$ *parametric domain.*

We finally develop some ideas in the following borrowing from the implicit function theorem in order to study the smoothness and stability transition behavior around the ζ_0 curve in (h, δ) domain.

4.3. Local vs. global characterization. We elaborate on the geometry of ζ_0 from the implicit function theorem [14], which states that, on the imaginary axis, the characteristic equation $a(s, h, \delta)|_{s=j\omega} = H_i(j\omega)\Delta(j\omega) - 1 = 0$ may be used to locally express h and δ in terms of ω as an implicit function, in the form of $(h, \delta) = \varphi(\omega)$, if $da/d\omega \neq 0$ holds. This condition is nothing but the definition of the existence of *regular points* that allows the implementation of the implicit function theorem locally.

By the help of the interconnection scheme interpretation and the monotonicity ideas, the local representation can be extended. Following the theorem, one first classifies the points on ζ_0 in the (h, δ) domain. Such a classification identifies whether the implicit function theorem is applicable or not on the function $a(s, h, \delta) = 0$. Parameter δ is continuous on ζ_0, and its variation with respect to k is nonzero. Similar arguments also hold for h; see Proposition 4.6). The smoothness and nonzero derivative of the variables h on ζ_0 indicate that ζ_0 consists of only "regular points." This suffices to show that the theorem is applicable around *any* local point of ζ_0. By introducing the variable u along with the interconnection scheme, which only scales ω, we manage to separately express $h = \varphi_1(u)$ and $\delta = \varphi_2(u)$ *globally* on the stability boundary ζ_0.

So far we have shown the existence and the geometry of the stability region connected to the origin of the parametric domain (h, δ), intersecting the h and δ axis. In the following, the characterization of the stability/instability transition of the dynamics in (h, δ) using (4.2) is presented. For this objective, we use the idea based on the implicit function theorem [9], along with the separation of variables h and δ via the interconnection scheme that we have considered.

Take the characteristic equation $a(s, h, \delta) = H_i\Delta - 1 = 0$. When s moves along the imaginary axis, an (h, δ) pair moves along $\zeta_0(h, \delta)$. Let us first define the following for a given $\omega \in \Gamma_\omega$ on the $\zeta_0(h, \delta)$ curve:

$$R_0 = \Re\left(\frac{j}{s}\frac{\partial a(s,h,\delta)}{\partial s}\right)_{s=j\omega}, \quad R_1 = -\Re\left(\frac{1}{s}\frac{\partial a(s,h,\delta)}{\partial h}\right)_{s=j\omega},$$

$$I_0 = \Im\left(\frac{j}{s}\frac{\partial a(s,h,\delta)}{\partial s}\right)_{s=j\omega}, \quad I_1 = -\Im\left(\frac{1}{s}\frac{\partial a(s,h,\delta)}{\partial \tau_\nu}\right)_{s=j\omega},$$

$$R_2 = -\Re\left(\frac{1}{s}\frac{\partial a(s,h,\delta)}{\partial \delta}\right)_{s=j\omega}, \quad I_2 = -\Im\left(\frac{1}{s}\frac{\partial a(s,h,\delta)}{\partial \delta}\right)_{s=j\omega}.$$

By Lemma 4.1, $a(s,h,\delta)=0$ is an analytical function, and using the implicit function theorem, the tangent of $\zeta_0(h,\delta)$ is expressed as

$$\begin{pmatrix} dh/d\omega \\ d\delta/d\omega \end{pmatrix} = \begin{pmatrix} R_1 & R_2 \\ I_1 & I_2 \end{pmatrix}^{-1} \begin{pmatrix} R_0 \\ I_0 \end{pmatrix} = \frac{1}{R_1I_2 - R_2I_1} \begin{pmatrix} R_0I_2 - I_0R_2 \\ I_0R_1 - R_0I_1 \end{pmatrix}, \tag{4.27}$$

provided that $R_1I_2 - R_2I_1 \neq 0$. In order to characterize the stability transition, one needs to consider h and δ as functions of $s=\mu+j\omega$. Since the tangent of $\zeta_0(h,\delta)$ along the positive direction (i.e., increasing ω direction) is $(dh/d\omega, d\delta/d\omega)$, the normal to the $\zeta_0(h,\delta)$ curve pointing to the left-hand side of the positive direction is $(-d\delta/d\omega, dh/d\omega)$. Also, as a pair of complex conjugate roots of $a(s,h,\delta)=0$ crosses the imaginary axis at $s=j\omega$ to $\mathbb{C}_+$, (h,δ) moves along the direction $(\partial h/\partial\mu, \partial\delta/\partial\mu)$. So, if the inner product of this vector with the normal vector is positive, i.e.,

$$\left(\frac{\partial h}{\partial\omega}\frac{\partial\delta}{\partial\mu} - \frac{\partial\delta}{\partial\omega}\frac{\delta h}{\partial\mu}\right)_{s=j\omega} > 0, \tag{4.28}$$

then the region on the left of the stability curve $\zeta_0(h,\delta)$ at $s=j\omega$ has two more unstable roots than the right of $\zeta_0(h,\delta)$ curve. On the other hand, if the inner product is negative, then the region on the left of the stability curve $\zeta_0(h,\delta)$ has two fewer unstable roots than the region on its right. Similar to the tangency condition defined in (4.27), we can express $(\partial h/\partial\mu, \partial\delta/\partial\mu)$ as in the following:

$$\begin{pmatrix} \partial h/\partial\mu \\ \partial\delta/\partial\mu \end{pmatrix} = \begin{pmatrix} R_1 & R_2 \\ I_1 & I_2 \end{pmatrix}^{-1} \begin{pmatrix} I_0 \\ -R_0 \end{pmatrix} = \frac{1}{R_1I_2 - R_2I_1} \begin{pmatrix} R_0R_2 + I_0I_2 \\ -R_0R_1 - I_0I_1 \end{pmatrix}. \tag{4.29}$$

PROPOSITION 4.15. *Given any (h,δ) pair on the stability curve $\zeta_0(h,\delta)$, the inequality* (4.28) *is always satisfied.*

Proof. Simple manipulations show that $\left(\frac{\partial h}{\partial\omega}\frac{\partial\delta}{\partial\mu} - \frac{\partial\delta}{\partial\omega}\frac{\delta h}{\partial\mu}\right)_{s=j\omega} > 0$ if

$$R_2I_1 - R_1I_2 = \left(\frac{|\lambda_i|}{\omega}\right)^2 \frac{4\sin^2(\delta\omega/2) - \delta\omega\sin(\delta\omega)}{(\delta\omega)^3} > 0. \tag{4.30}$$

As per (4.7) and from Proposition 4.6, for $u\in(0,\pi/2)$, the inequality in (4.30) can be alternatively studied over

$$2\sin^2(u) - u\sin(2u) > 0, \quad u\neq 0. \tag{4.31}$$

This inequality always holds since it can be rewritten in the form of a well-known trigonometric property, $\sin(u)/u > \cos(u)$, in the interval $u\in(0,\pi/2)$. For the case when $u=0$, we state that f_Δ is continuous and its derivative exists at $u=0$; therefore similar arguments on the smoothness of ζ_0 hold for $u=0$ as well. ∎

REMARK 4.16. *Since the region below ζ_0 is known to be stable, Proposition* 4.15 *indicates that the region on the other side of ζ_0 has two unstable roots. Also, with the above proof, the smoothness of the stability curve ζ_0 is guaranteed.*

γ-distribution with and without a gap. We finally comment on the γ-distribution with and without gap. By (4.5), the characteristic equation is

$$s(qs+1)^p - e^{-hs}\lambda_i = 0. \tag{4.32}$$

When $h=0$, the above equation becomes a polynomial in s whose stability is easy to determine. At the origin of the parameter domain $(p,q)=(0,0)$, the characteristic

equation becomes $s - \lambda_i = 0$, which is stable by Lemma 4.1. For $p \neq 0$ or $q \neq 0$, the stability can be studied by numerical computation of the roots or by using the jury test. In the example case studies, we will study the stability of (4.32) via numerical computations.

When the γ-distribution has a positive gap h, the analysis is more complicated. In the parametric domain of (p, q), the problem reduces to assuring the stability of the dynamics (2.2) with respect to λ_i and gap h. We study the stability in the (h, q) parametric domain by taking fixed p values. The procedure is as follows. Using the fact that eigenvalues of J are in complex conjugate pairs, one can reform the characteristic equation directly from (3.8) with real coefficients and perform the stability analysis for various selections of fixed p in the domain of (h, q). We mention that there exist various techniques in the literature to handle this analysis [17, 10, 22, 24].

5. Illustrative examples. In the following, some example cases are presented to demonstrate the memory effects on the stability of traffic flow dynamics and their physical interpretations. The developed theory equally allows one to study various scenarios such as the influence of the number of vehicles, presence of nonidentical drivers, aggressiveness of drivers, etc. In order to preserve coherence among the example cases, we will present the case when the drivers are identical (thus $\kappa_i = \kappa$) and compare the arising stability features of traffic dynamics with respect to aggressiveness of the drivers κ and the two spatial configurations given in Figure 2.2.

5.1. Uniform distribution. We take $\kappa_i = \kappa = 1.5$ and $\kappa_i = \kappa = 2$, respectively, which are in the same order of magnitude with those given in [2]. Figure 5.1(a) depicts the stability region for the ring configuration. The region shaded by light gray, Φ_1, represents the stability domain when $\kappa = 2$. When $\kappa = 1.5$, the stability region is enlarged by an additional region labeled as Φ_2 (dark grey); hence $\Phi_1 \cup \Phi_2$ becomes the stability region.

From Figure 5.1(a) we conclude that for both κ values the size of the memory window that is "tolerable" (to maintain stability) is the widest when $h = 0$. With a nonzero dead-time ($h \neq 0$) the allowable window size becomes narrower and eventually disappears.

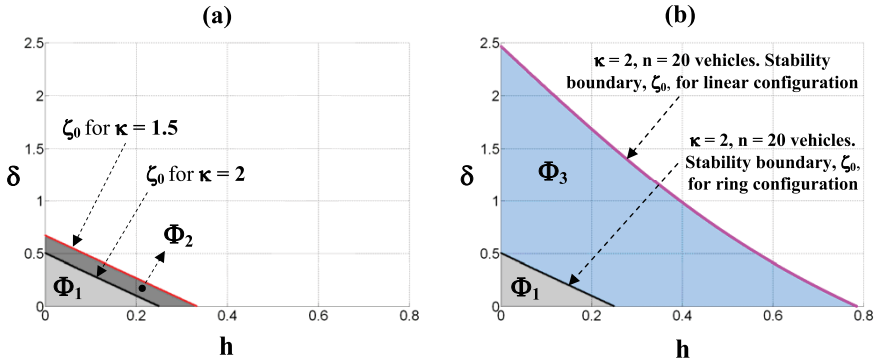

FIG. 5.1. (a) *The size of the memory window δ (sec) versus h (sec) for the system* (2.2) *with uniformly distributed delays* (2.3) *and $n = 20$ vehicles. The shaded area is the stability region.* (b) *Comparison of stability regions for ring and linear spatial configuration of vehicles, with $\kappa = 2$ and $n = 20$ vehicles.*

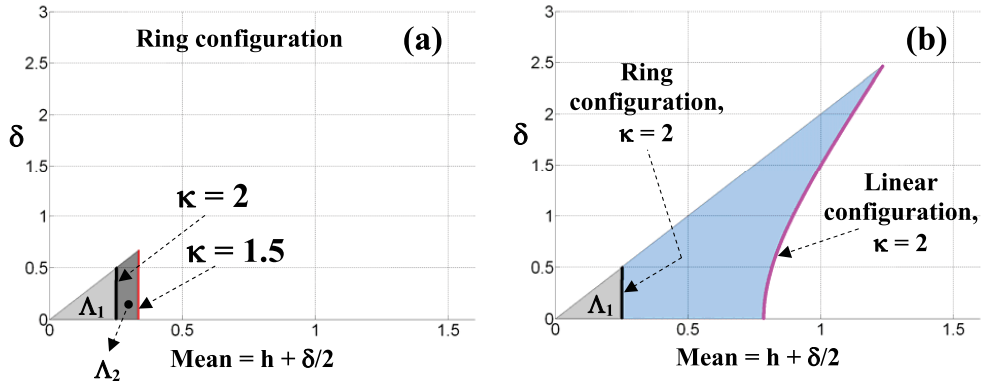

FIG. 5.2. *Stability regions in the parameters mean delay and memory size, for $n = 20$ vehicles.* (a) *Ring configuration for $\kappa = 1.5$ and $\kappa = 2$,* (b) *comparison between linear and ring configurations with $\kappa = 2.0$.*

5.1.1. Stability regions for ring and linear configurations. We now compare the stability regions for the different spatial configurations of the vehicles depicted in Figure 2.2. Figure 5.1(b) compares the stability regions for $n = 20$ vehicles. The regions labeled by Φ_1 in subfigures (a) and (b) are identical. Thus, the linear configuration offers an enhancement in the stability by the additional Φ_3 region.

The stability enhancement in the linear configuration can be explained mathematically. In a global sense, one can state a measure of the stability enhancement by how large $\bar{h}$ and $\bar{\delta}$ are. This can be easily checked by the results in Proposition 4.3. By Lemma 3.1, the eigenvalues of the configuration matrix J' are real in the linear configuration, implying $\phi = \pi$. For this setting of ϕ, it can be verified from (4.14) that $\bar{h}$ and $\bar{\delta}$ attain their maximum values: $\bar{h} = \frac{\pi}{2\kappa_{\max}}$ and $\bar{\delta} = \frac{\pi^2}{2\kappa_{\max}}$. This can be proven by assuming identical drivers with special form of λ_i as per (3.5), which can be used in (4.14) to show that as $\phi \to \pi$, the stability margins increase on both h and δ axes.

Physically, the linear configuration represents more degrees of freedom in the coupled dynamics, since the leading car is not restricted by the traffic, whereas in the ring configuration the motion of each vehicle plays a role in determining stability, thus limiting larger stability regions.

5.1.2. Stability with respect to mean delay versus memory size. We now present stability regions in the parameter domain *mean delay* $(h+\delta/2)$ versus *memory size* (δ). The mean of the uniform distribution represents the averaged effects of the memory, and it converges to the discrete delay case as the memory size approaches zero. Hence, the mean can also be seen as a link from discrete to distributed delays.

The traffic scenario is the same as in section 5.1. We first take a ring configuration of $n = 20$ vehicles with identical drivers and depict the stability regions in the new parametric domain. Thus, the stability pictures in Figure 5.1(a) correspond to those in Figure 5.2(a). The region Φ_1 is distorted in the new domain, $h \times \delta \to (h + \delta/2) \times \delta : \Phi_1 \mapsto \Lambda_1$, and similarly $(\Phi_1 \cup \Phi_2) \mapsto (\Lambda_1 \cup \Lambda_2)$. Figure 5.2(b) compares the stability regions for the ring and linear configurations, for $\kappa = 2.0$. The labeled regions correspond to those in Figure 5.1(b) as $\Phi_1 \mapsto \Omega_1$, and $(\Phi_1 \cup \Phi_2) \mapsto (\Omega_1 \cup \Omega_2)$.

Figure 5.2(a) shows how overaggressive drivers (large κ) cause instability, unless

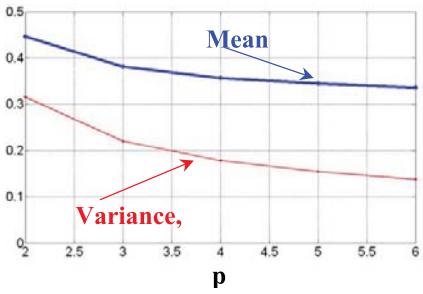

FIG. 5.3. (a) *Maximum allowable mean delay and the corresponding variance of the γ-distribution ($h = 0$) for varying p values.* (b) *Crossing boundary in mean vs. variance of the γ-distribution ($h = 0$).*

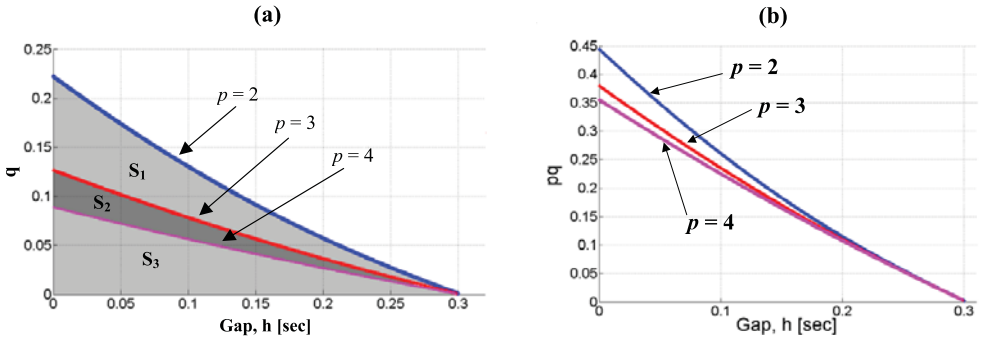

FIG. 5.4. (a) *Stability regions in (h, q) domain for various values of the parameter p of the γ-distribution with gap.* (b) *Corresponding stability boundaries in (h, pq) domain.*

the mean delay and the memory window are reduced, i.e., they can react almost instantaneously. This is analogous to feedback control systems where high gains may cause instability. Figure 5.2(b) shows that the linear configuration of the vehicles allows larger memory windows that can be utilized by the drivers without inducing instability. For this particular example, the allowable memory size (that preserves stability) in linear configuration of the vehicles is five times more than that of the ring configuration. An interesting observation from Figure 5.2(b) is that if the mean delay is relatively large (e.g., $h + \delta/2 = 1$ in linear configuration), stability is still possible, but too small or too large window sizes yield instability. In contrast, for smaller values of mean delay, the window size can even become zero, resuming the discrete delay case. This clearly shows the nontrivial qualitative effects of distributed delays.

5.2. γ-distribution with and without gap. We consider $n = 3$ vehicles and identical drivers with $\kappa = 2$. For $h = 0$ and $p \in [2, 6]$, we identify the maximum allowable q for which the characteristic equation (4.32) remains stable. Using these q values, the mean pq and the variance pq^2 of the distribution are plotted with respect to the parameter p in Figure 5.3. Notice that for smaller p the variance becomes larger, which corresponds to larger mean delay. This is also an indication of larger stability regions. In other words, increasing the variance of the delay distribution for a fixed mean delay enlarges the stability region.

In the case of a nonzero gap h, i.e., in the presence of a dead-time, the stability regions are shown in Figure 5.4(a) as p values. The shaded zones S_3, $S_2 \cup S_3$, and

$S_1 \cup S_2 \cup S_3$ correspond to stability regions for $p = 4$, $p = 3$, and $p = 2$, respectively. The subplots in Figure 5.4 have the same color coding. Note that the influence changing p on the stability region is more pronounced for small values of h than for larger values. We emphasize that, when modeling memory effects, the presence of a gap may not be negligible since the dynamics may become sensitive even to a small gap.

6. Conclusions. We have studied the stability of a single-lane microscopic car-following model in the parametric domain describing the delayed reactions of human drivers. In contrast to the literature, we have modeled such delayed reactions based on the "memory capabilities" of human drivers, which assumes that control actions are based on a "memory window" distributed over the the time history of the traffic flow dynamics. The resulting system with distributed delays offers a more realistic model, although the corresponding stability analysis becomes more difficult. In the analytical development of the paper, we have derived necessary and sufficient conditions for the stability of the traffic flow with distributed delays. Numerical examples have been given for two common delay distributions, two spatial configurations, and a realistic set of parameter values. The results show some nontrivial effects of distributed delays and reiterate that the modeling and analysis of traffic holds many mathematical challenges.

Acknowledgments. Part of this work was conducted at HeuDiaSyC (UMR CNRS 6599), Compiègne, France, in the academic year 2005–2006, during which Rifat Sipahi was supported by the Chateaubriand Scholarship of the French Government. R.S. and S.-I.N. are grateful to Martin Treiber, T.U. Dresden, Germany, for fruitful discussions on the dynamics of traffic flow, and acknowledge the financial support of Centre National de Recherche Scientifique (CNRS) for R.S.'s visit to F. M. Atay at Max Planck Institute on distributed delays and memory effects.

REFERENCES

[1] F. M. Atay, *Distributed delays facilitate amplitude death of coupled oscillators*, Phys. Rev. Lett., 91 (2003), paper 094101.
[2] M. Bando, K. Hasebe, K. Nakanishi, and A. Nakayama, *Analysis of optimal velocity model with explicit delay*, Phys. Rev. E, 58 (1998), pp. 5429–5435.
[3] E. Beretta and Y. Kuang, *Geometric stability switch criteria in delay differential systems with delay dependent parameters*, SIAM J. Math. Anal., 33 (2002), pp. 1144–1165.
[4] R. E. Chandler, R. Herman, and E. W. Montroll, *Traffic dynamics: Analysis of stability in car following*, Oper. Res., 7 (1958), pp. 165–184.
[5] R. Datko, *A procedure for determination of the exponential stability of certain differential-difference equations*, Quart. Appl. Math., 36 (1978), pp. 279–292.
[6] L. C. Davis, *Modifications of the optimal velocity traffic model to include delay due to driver reaction time*, Phys. A, 319 (2003), pp. 557–567.
[7] M. Green, *"How long does it take to stop?" Methodological analysis of driver perception-brake times*, Transportation Human Factors, 2 (2000), pp. 195–216.
[8] H. Greenberg, *An analysis of traffic flow*, Oper. Res., 7 (1959), pp. 78–85.
[9] K. Gu, S.-I. Niculescu, and J. Chen, *On stability crossing curves for general systems with two delays*, J. Math. Anal. Appl., 311 (2005), pp. 231–253.
[10] K. Gu, V. L. Kharitonov, and J. Chen, *Stability of Time-Delay Systems*, Birkhäuser Boston, Cambridge, MA, 2003.
[11] J. K. Hale and W. Huang, *Global geometry of the stable regions for two delay differential equations*, J. Math. Anal. Appl., 178 (1993), pp. 344–362.
[12] D. Helbing, *Traffic and related self-driven many-particle systems*, Rev. Modern Phys., 73 (2001), pp. 1067–1141.
[13] A. R. Horn and C. R. Johnson, *Matrix Analysis*, Cambridge University Press, Cambridge, UK, 1985.

[14] G. Iooss and D. D. Joseph, *Elementary Stability and Bifurcation Theory*, Undergrad. Texts in Math., Springer-Verlag, New York, 1980.
[15] W. Michiels and S.-I. Niculescu, *Stability and Stabilization of Time-Delay Systems: An Eigenvalue-Based Approach*, Adv. Des. Control 12, SIAM, Philadelphia, 2007.
[16] R. M. Murray, ed., *Control in an Information Rich World: Report of the Panel on Future Directions in Control, Dynamics, and Systems*, SIAM, Philadelphia, 2003.
[17] S.-I. Niculescu, *Delay Effects on Stability: A Robust Control Approach*, Lecture Notes in Control and Inform. Sci. 269, Springer-Verlag, Heidelberg, 2001.
[18] G. Orosz and G. Stepan, *Hopf bifurcation calculations in delayed systems with translational symmetry*, J. Nonlinear Sci., 14 (2004), pp. 505–528.
[19] G. Orosz, R. E. Wilson, and B. Krauskopf, *Global bifurcation investigation of an optimal velocity traffic model with driver reaction time*, Phys. Rev. E, 70 (2004), paper 026207.
[20] G. Orosz, B. Krauskopf, and R. E. Wilson, *Bifurcations and multiple traffic jams in a car-following model with reaction time delay*, Phys. D, 211 (2005), pp. 277–293.
[21] R. W. Rothery, in Traffic Flow Theory, 2nd ed., TRB Special Report Volume 165, N. H. Gartner, C. J. Messner, and A. J. Rathi, eds., Transportation Research Board (TRB), Washington, DC, 1992, Chapter 4.
[22] R. Sipahi and N. Olgac, *Complete stability robustness of third-order LTI multiple time-delay systems*, Automatica, 41 (2005), pp. 1413–1422.
[23] R. Sipahi and S.-I. Niculescu, *Analytical stability study of a deterministic car following model under multiple delay interactions*, in Proceedings of the 6th IFAC Time Delay Systems Workshop, L'Aquila, Italy, 2006, International Federation of Automatic Control/Elsevier, Oxford, UK, 2006.
[24] G. Stepan, *Retarded Dynamical Systems: Stability and Characteristic Function*, Longman Scientific & Technical/John Wiley & Sons, New York, 1989.
[25] O. Toker and H. Ozbay, *Complexity issues in robust stability of linear delay-differential systems*, Math. Control Signals Systems, 9 (1996), pp. 386–400.
[26] M. Treiber and D. Helbing, *Memory effects in microscopic traffic models and wide scattering in flow-density data*, Phys. Rev. E, 68 (2003), paper 046119.
[27] M. Treiber, A. Kesting, and D. Helbing, *Delays, inaccuracies and anticipation in microscopic traffic models*, Phys. A, 360 (2006), pp. 71–88.